Available online at www.sciencedirect.com
ScienceDirect
Ceramics International 35 (2009) 1595–1601
CERAMICS INTERNATIONAL
www.elsevier.com/locate/ceramint

Effect of storing on the microstructure of Ag/Cu/HA powder

Hui Yang [a,b], Lin Zhang [b], Ke-Wei Xu [a,*]

[a] State Key Laboratory for Mechanical Behavior of Materials, Xi'an Jiaotong University, Xi'an 710049, PR China
[b] Life College of Science & Engineering, Shaanxi University of Science & Technology, Xi'an weiyang district university park 710021, PR China

Received 21 August 2007; received in revised form 21 May 2008; accepted 1 September 2008
Available online 14 October 2008

Abstract

The nanosized Ag/Cu/HA powder is thermodynamically unstable and easily congregates during storing, which may make it lose the nanomaterial's properties. In this work, the performances of Ag/Cu/HA during storing were studied. The Ag/Cu/HA powders were prepared using a one-step co-precipitation method. The effects of storing on powder microstructures were investigated. The microstructures of Ag/Cu/HA powders were characterized by X-ray diffraction and scanning electron microscopy. The results show that the diffraction intensities and the sizes of the calcined Ag/Cu/HA powders are reduced during storing. Storing makes the diffraction angles of 0 0 2 and 3 0 0 peaks decreased and makes that of 2 1 1 peak increased. In addition, storing increases the crystal growth along the *c*-axis without the effect on the crystal morphology of powders. The stored Ag/Cu/HA powders can induce the formation of new HA crystal the same as the stored Ag/Cu/HA powders with platelet morphology and low intensity and crystallinity similar to nature bone.

Keywords: A. Powders: chemical preparation; B. Nanocomposites; C. Chemical properties; D. Apatite

1. Introduction

The predominant purpose of biomaterials is to produce a part or facilitate a function of the human body in a safe, reliable, economical, and physiologically acceptable manner [1] without producing an inflammatory tissue reaction. Accordingly, hydroxyapatite (HA) and its composites, which have been extensively proposed as implants for bone-repairing and tissue engineering scaffold, must have acceptable biocompatibility and mechanical performances. Previous experiments have revealed that biological performances of HA implants were closely related to their phase compositions and microstructures [2–10]. It was reported that the long and thin shape as well as the parallel distribution of the hydroxyapatite sheets in the shankbone improves the maximum pullout force of the sheets and the fracture toughness of the bone [11]. Kaneko et al. [12] found that the mouse fibroblasts (L929) extended onto the oriented HA–hydrogel hybrid along the drawing direction, which may lead to the development of a tissue engineering scaffold for yielding oriented bony tissues.

The transition metallic silver ion (Ag^+) and copper ion (Cu^{2+}) have stronger antibacterial properties than any other metallic ions. The antimicrobial properties of Ag^+ have been exploited for a long time in the biomedical field [13]. The significant feature of Ag^+ is its broad-spectrum antimicrobial property, which is particularly significant for the polymicrobial colonization associated with biomaterials infection [14]. The antimicrobial properties of Cu^{2+} are inferior to Ag^+, however, more effective against *mold* than Ag^+. The HA containing Ag^+ (Ag/HA) and HA containing Cu^{2+} (Cu/HA) have been made and confirmed to have good antibacterial properties [15–19]. Sutter et al. [20] investigated the properties of the Cu/HA crystal and the results show that it has a smaller dissolution rate than pure HA. Kim et al. [21] also synthesized the Ag/HA and Cu/HA powders and proved their effective antibacterial property. Therefore, the nanosized Ag/Cu/HA may be a good biomaterial in antibacterial property and biocompatibility as it has two functional metal ions.

The nanosized Ag/Cu/HA powder, however, is thermodynamically unstable and may congregate to form large particles during storing. This may make the microstructures of Ag/Cu/HA powder changed and lose its nanomaterial properties such as the ability to enhance the adhesion and strength of coating when it is used in coating. In previous experiments the

* Corresponding author. Tel.: +86 29 88403018; fax: +86 29 3237910.
E-mail address: kwxu@mail.xjtu.edu.cn (K.-W. Xu).

0272-8842/$34.00 © 2009 Published by Elsevier Ltd and Techna Group S.r.l.
doi:10.1016/j.ceramint.2008.09.012

microstructure changes of Ag/Cu/HA powder during storing were not studied. In this work the nanosized Ag/Cu/HA powders were prepared using a one-step co-precipitation method which yielded flower petal crystals. Previously synthesized Ag/Cu/HA crystals had needle or rod shapes. The obtained powder in this study was calcined at temperatures from 300 to 600 °C and stored at room temperature for 4 months. The effects of storing on the microstructure of the nanosized Ag/Cu/HA powder calcined were investigated.

2. Experimental

The raw Ag/Cu/HA powder was prepared using a one-step co-precipitation and the atom ratio of Ca to P in the solution of reaction was set to 1.67. The 0.1 mol/L $(NH_4)_2HPO_4$, during the reaction, was slowly added into the solution of 0.1 mol/L $Ca(NO_3)_2$ with specific amount of $AgNO_3$ and $Cu(NO_3)_2$ by stirring rapidly. This resulted in the formation of a Ag/Cu/HA slurry. The slurry was heated in 100 °C water-bath for 4 h with rapid stirring so as to obtain perfect crystalline, then aged for 24 h and after that filtrated in vacuum. The collected wet Ag/Cu/HA powders were dried at 100 °C for 24 h, then slowly cooled within the kiln to room temperature. Next, two samples of as-produced Ag/Cu/HA powder were heated to 300 and 600 °C respectively, held for 2 h and then slowly cooled back to room temperature in the furnace. The heating and cooling were performed in air atmosphere. Finally the as-calcined Ag/Cu/HA powder samples were stored in a desiccator at room temperature for 4 months. The composition of investigated Ag/Cu/HA powder was analyzed by X-ray diffraction (XRD, D/max-2200PC). The operation conditions were 40 KV × 40 mA, DS-RS-SS = 1°-0.3 mm-1° by using CuKa. The goniometer was set at a scan rate (2θ) of 16°/min over a range (2θ) of 10–80° and at a step size of 0.02°. Surface morphology of the investigated Ag/Cu/HA powder was observed by scanning electron microscopy (SEM, JEOL 6700F). The size of the Ag/Cu/HA powder was calculated using the XRD data.

The antibacterial property of the Ag/Cu/HA powder dried at 100 °C was tested with minimum inhibitory concentrations (MIC) method. Firstly, 0.1–0.2 g Ag/Cu/HA powder was added into 100 ml liquid-casein–agar-culture by stirring and secondly, the obtained culture was diluted with the same liquid-casein–agar-culture to get various concentration cultures with the Ag/Cu/HA powder. Then, *E. coli.* and *S. mutans* ATCC 25175 were inoculated in the various obtained cultures respectively. Next, the inoculated cultures were put into the culture box and cultured for 24 h and meantime the blank culture without any bacteria was also put into the culture box as a comparison sample. After that, the various cultures were observed and the least concentration of Ag/Cu/HA powder, with it the culture could not grow any bacteria the same as the blank culture did, is the MIC of the Ag/Cu/HA powder.

Ag/Cu/HA powder was pressed into pellets with a of diameter 10 mm, thickness 4 mm at 15 MPa, then the pellets were immersed in simulated body fluid (SBF) for 18 days and during immersing of them, SBF was replaced every three days. After that, the immersed Ag/Cu/HA pellets were softly washed with distilled water. Finally the washed test samples were dried at 100 °C for 24 h and stored in a desiccator waiting for characterization.

3. Results and discussion

3.1. XRD analysis

During storing the calcined Ag/Cu/HA crystal becomes more stable and its crystallization reaches to the thermodynamic equilibrium state. In the process the inherent energy of the crystal, related closely with its microstructure will be changed, therefore storing can change the microstructure of the calcined Ag/Cu/HA crystal. Figs. 1 and 2 show the XRD patterns of the calcined Ag/Cu/HA powders and Tables 1 and 2

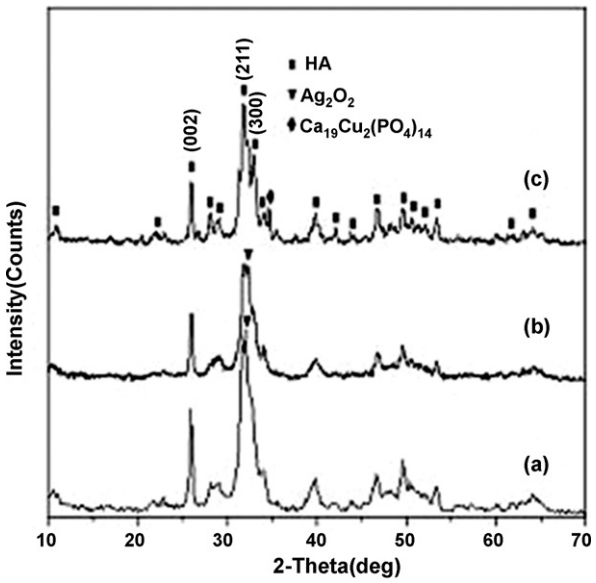

Fig. 1. The XRD patterns of the calcined Ag/Cu/HA powders at (a) 100 °C, (b) 300 °C and (c) 600 °C before storing.

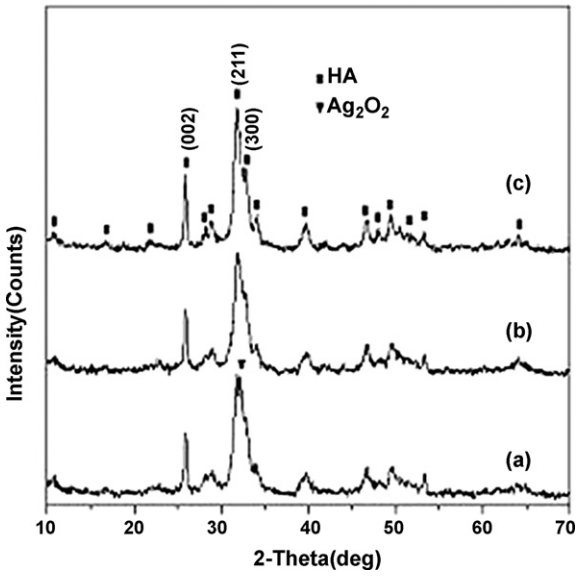

Fig. 2. The XRD patterns of the calcined Ag/Cu/HA powders at (a) 100 °C, (b) 300 °C and (c) 600 °C after storing.

Table 1
Peak displacement (*P.D.*), intensity (*I*) and particle size (*s*) of Ag/Cu/HA powders heated at various temperatures before storing.

Temperature/°C	0 0 2			3 0 0			2 1 1		
	I/count s^{-1}	*s*/nm	*P.D.*/(°)	*I*/count s^{-1}	*s*/nm	*P.D.*/(°)	*I*/count s^{-1}	*s*/nm	*P.D.*/(°)
100	127	24.1	−0.001	81	34.2	0.032	195	9.0	0.093
300	78	26	−0.061	49	34.7	−0.108	125	8.7	−0.007
600	74	25.8	−0.061	92	18.4	0002	163	10.7	−0.027

Table 2
Peak displacement (*P.D.*), intensity (*I*) and particle size (*s*) of Ag/Cu/HA powders heated at various temperature after storing.

Temperature/°C	0 0 2			3 0 0			2 1 1		
	I/count s^{-1}	*s*/nm	*P.D.*/(°)	*I*/count s^{-1}	*s*/nm	*P.D.*/(°)	*I*/count s^{-1}	*s*/nm	*P.D.*/(°)
100	47	204	−0.060	33	27.3	0.054	94	3.6	0.032
300	50	25.3	−0.021	42	30.9	0.032	36	3.6	−0.047
600	64	24.8	0037	45	15.9	0.004	105	10.4	−0.087

Table 3
The peak displacement of Ag/Cu/HA powders heated at various temperature and the changes of diffraction intensity and particle size (Δ*I*, Δ*P.D.* and Δ*s*) between before and after storing.

Temperature/°C	0 0 2			3 0 0			2 1 1		
	Δ*I*/count s^{-1}	Δ*s*/nm	Δ*P.D.*/(°)	Δ*I*/count s^{-1}	Δ*s*/nm	Δ*P.D.*/(°)	Δ*I*/count s^{-1}	Δ*s*/nm	Δ*P.D.*/(°)
100	80	3.7	0.059	43	6.9	0.022	101	04	0.061
300	28	0.2	−0.040	7	3.8	−0.140	39	0.1	0.040
600	10	1.0	−0.098	46	2.5	−0.002	58	0.3	0.060

present the lattice parameters of the Ag/Cu/HA powder before and after storing respectively. Results indicate that the diffraction intensity of the calcined Ag/Cu/HA powder before storing decreases as the calcination temperature increases from 100 to 600 °C (see Table 1). However, after storing the tendency is changed as shown in Table 2, the higher the calcinations temperatures are, the stronger the diffraction intensities of 0 0 2, 3 0 0 and 2 1 1 peaks.

Table 3 shows the peak displacements of the stored Ag/Cu/HA powders heated at various temperatures, and the changes of diffraction intensity and particle size (Δ*P.D.*, Δ*I* and Δ*s*). Based on the data in Table 3 we can draw the conclusion that storing makes the intensities of peaks reduced significantly and the changes of the 0 0 2 intensity are progressively lowered as the temperature rises. The reductions of the diffraction intensity and the diffraction angle indicate the decrease of the crystallinity and expansion of the lattice space respectively. As a result, the stored crystals have larger dissolution rate than the un-stored crystal [22]. This makes the stored crystal more similar to nature bone which has a low crystallinity. The most obvious intensity reduction is observed in the sample dried at 100 °C, implying the Ag/Cu/HA powder calcined at a low temperature has a poor stability during storing at room temperature and has a low crystallinity after storing.

3.2. Microstructure change and ion polarization

According to the theory of ion polarization, cations especially the transition-metal ions with smaller radii and higher positive charges, such as Ag^{+}, Cu^{2+} and La^{3+}, have the ability to change the electronic distribution of anions contacted with them, especially the anions with larger radii and more negative charges, such as I^{-}, PO_4^{3-}. Furthermore, cations and anions influence each other, resulting in the formation of an extra-polarization which further intensifies the connection between them. Consequently, the distances between cations and anions become shorter and shorter until they reach the thermodynamic equilibrium state. The relationship between the distance (r_0) of cation to anion and polarization energy (*Up*) is as follows:

$$Up = -\frac{NBe^2(Z^*a_{--} + Z^*a_{-+})}{2r_0^4} \quad (1)$$

where *B* is a coefficient, $1/(4\pi)$ usually suitable to various compounds; *N* is Avogadro's number, 6.02×10^{23}; Z^*_+, Z^*_-, a_+, and a_- are the effective charges and the polarizability of positive and negative ions respectively [23]. This formula fits to all ionic crystalline. For a given ionic compound, all of *N*, *B*, *e*, Z^*_+, Z^*_-, a_{-+}, and a_- are constants, so the polarization energy *Up* is inversely proportional to r_0^4, implying strong polarization can make r_0 short.

Up is a kind of inherent energy because it describes the interaction of ions in a molecule. Temperature is a key factor affecting the movement of electrons in an ion and in turn affecting the value of polarizability of it. Therefore, the polarization is substantially controlled by the system temperature according to Eq. (1). The higher the temperature

is, the stronger the polarization. So, the Ag/Cu/HA powder stored at room temperature for 4 months should have weaker polarization than it is at the temperature of 100 °C, meaning that the crystal has larger lattice space (*d*) at room temperature which results in the reduction of diffraction angle. Table 3 shows that storing basically makes the diffraction angle of 0 0 2 and 3 0 0 peak decreased and makes that of the 2 1 1 peak increased, indicating that the crystal lattice space(*d*) of either 0 0 2 or 3 0 0 is expanded through storing, while that of 2 1 1 is contracted.

3.3. Size change

Thermodynamically, nanoparticles are often unstable and can spontaneously congregate during storing, resulting in size enlargement. Based on 0 0 2 and 2 1 1 planes, the particle sizes slightly change whereas based on 3 0 0 plane, the size is obviously reduced after storing (see Table 3). In addition, the change of particle size, during storing, based on 3 0 0, appears to be related to calcination temperature, the most significant size change is observed in the sample heated at 100 °C, similar to the results of 3.1 intensity analysis in the respect of change tendency.

Fig. 1 shows that at the high temperature of 600 °C, the $Ca_{19}Cu_2(PO_4)_{14}$ crystal can be formed and Fig. 2 indicates that at room temperature it can be decomposed and changed back to the original crystal, Ag and Cu-containing HA crystal. This means that energy should be provided during formation of $Ca_{19}Cu_2(PO_4)_{14}$ crystal and energy can be released leading to the damage of crystal in decomposition. Meantime, the crystal size is reduced and the reduction mainly occurs in the 3 0 0 plane (along *a*-axis), the same direction as that the Ag/Cu/HA lattice contracted when the $Ca_{19}Cu_2(PO_4)_{14}$ crystal formed at 600 °C (see Fig. 1 and discussion in Section 3.4).

Fig. 3 shows the FTIR spectra of the stored Ag/Cu/HA powders. The bands at 3443 and 1630 cm^{-1} indicate water is absorbed in the powders (see Fig. 3) (In fact, before storing the Ag/Cu/HA powders also contains very little water). Water cannot enter the lattice of HA crystal but it can hydrate the ions on the surface of the Ag/Cu/HA crystal, resulting in the formation of water layers around the Ag/Cu/HA particles which can make the small particle stable.

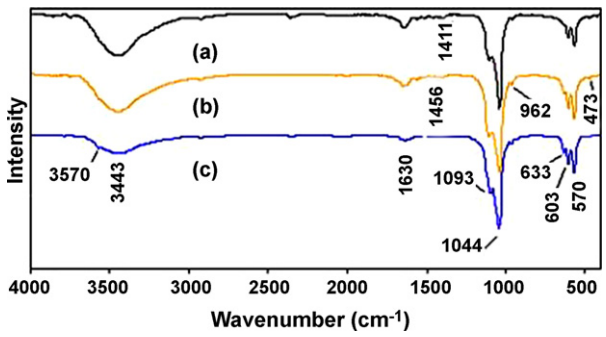

Fig. 3. FTIR spectra of the stored Ag/Cu/HA powders calcined at (a) 100 °C, (b) 300 °C and (c) 600 °C.

Table 4
Orientation parameter (*c*/*a*) of the Ag/Cu/HA powder heated at various temperature before and after storing.

Temperature/°C	*c*/*a* (before storing)	*c*/*a* (after storing)
100	0.7	0.75
300	0.75	0.83
600	1.40	1.56

3.4. Orientation growth

The value of *c*/*a* for the Ag/Cu/HA powder calcined at temperatures ranging from 100 to 600 °C before and after storing is summarized in Table 4, indicating that the value of *c*/*a* increases as the temperature rises. Storing also makes the value of *c*/*a* increased. The most obvious value change of *c*/*a* occurs in the sample calcined at 600 °C meaning that the Ag/Cu/HA preferentially grows along the *c*-axis at high temperature mainly due to the contracting of the 3 0 0 plane.

The orientation of the Ag/Cu/HA crystal is very important when it is used as biomaterials and there are many literatures related to the orientation of HA crystal. Kaneko's [12] studies confirmed that the mouse fibroblasts (L929) extended onto the oriented HA–hydrogel hybrid along the drawing direction, which may lead to the development of a tissue engineering scaffold for yielding oriented bony tissues. Shaw et al. [24] confirmed that orienting the charged COOH-terminal region of the amelogenin protein on the HA surface optimized to exert control on developing unusually long and highly ordered hydroxyapatite crystallites which constitute enamel. Rokita et al. [25] found the relationship between the preferential orientation of crystals and the mechanical loading of the structure. Kaneko et al. [12] successfully synthesized the *c*-axis of the HAP crystal cell oriented perpendicularly to the surface of the hydrogel.

3.5. SEM analysis

The SEM micrographs of the Ag/Cu/HA powders calcined at various temperatures before and after storing were obtained in this study and Fig. 4 only shows the ones after storing because the Ag/Cu/HA powders before storing almost have the same micrographs as that after storing. At 100 °C the crystal takes the shape of a 30–50 nm thick flower petal. The flower petal crystals are unrolled at the calcination temperature of 300 °C where the crystal takes the shape of a tree leaf, with surface area of 500 × 500–500 × 800 nm^2. The leaf crystal becomes incomplete and eyelets appear on the surface of powder calcined at 600 °C.

The stored Ag/Cu/HA powders obtained in this study are platelet/sheet crystals and with orient growth in the direction of *c*-axis similar to a nature bone which can enhance their biocompatibility and bioactivity. Many reports are associated to this study. Yamauchi's [26] research results indicated that the sheet HA crystal on the surface of a scaffold supported the attachment and growth of L929 fibroblast cells. Zhang et al. [27] proved that the sheet HA has excellent properties for cell attachment and proliferation. Chen et al. [11,28] conducted

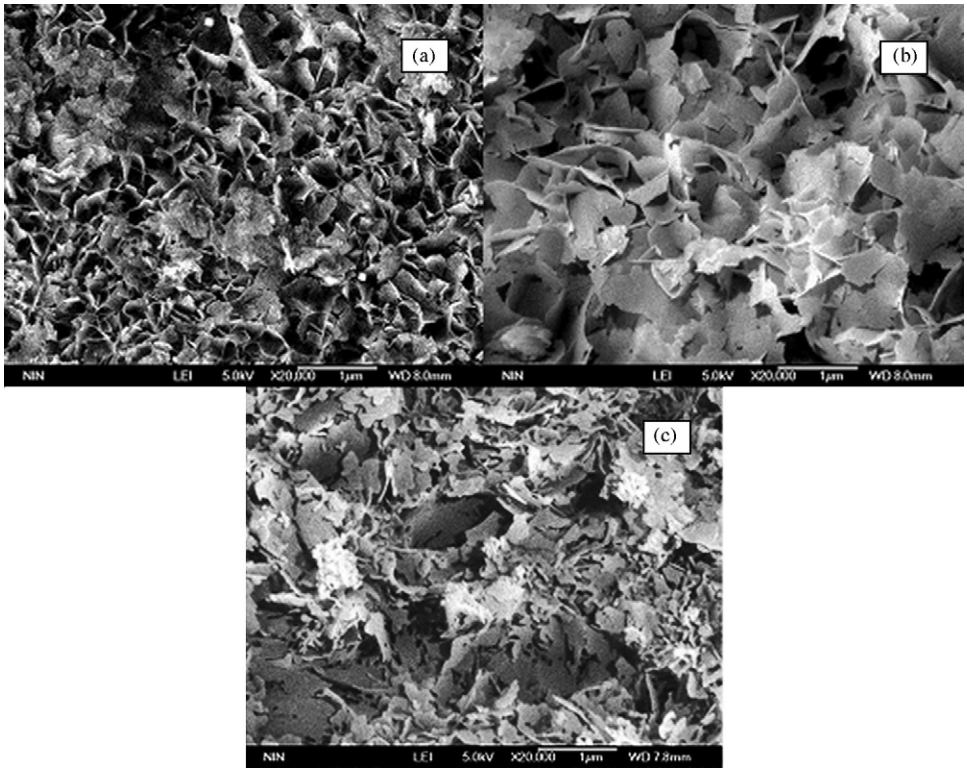

Fig. 4. The SEM micrographs of the Ag/Cu/HA powder calcined at (a) 100 °C, (b) 300 °C and (c) 600 °C after storing.

studies on the microstructure of a shinbone and a shankbone. Results show that each bone is a kind of natural bioceramic composite consisted of hydroxyapatite layers and collagen matrix. The hydroxyapatite layers consist of many hydroxyapatite sheets which are of thin and long shape and are arranged in a parallel distribution along the orientation of the maximum main stress of the bone. The long and thin shape as well as the parallel distribution of the hydroxyapatite sheets improves the maximum pullout force of the sheets and the fracture toughness of the bone. Accordingly, the increase of *c*/*a* value in the platelet Ag/Cu/HA crystal during storing can affect the formation of new HA and its oriented distribution when it is used as an implant.

3.6. Biocompatibility and antibacterial properties test

Ag^{+} and Cu^{2+} are transition metallic ions and have the ability to inhibit the propagation of bacteria or kill them because they can complex with chemical groups such as–NH_2, –S–S– and –CONH– of protein or enzyme in cells causing a damage of their DNA and RNA, when they are released from the Ag/Cu/HA crystal in body fluid. In addition, the Ag/Cu/HA powder has a large surface area as it is a nanosized particle, which makes bacteria adhere to the surface of the Ag/Cu/HA crystal. Table 5 presents the antibacterial test results of various HAs. The results prove that the doped HAs have effective antibacterial properties and the stored Ag/Cu/HA powder has the more effective antibacterial property than un-stored one and it is the most effective antibacterial materials in the five HAs listed by Table 5. This is because the stored powders have a lower crystallinity and larger dissolution rate than un-stored ones [22], as analyzed in Section 3.1.

Fig. 5 shows the SEM micrographs of the immersed Ag/Cu/HA pellets. Results indicate that new HA crystals were formed on the surface of the stored and the un-stored crystal pellets during immersing in SBF compared with Fig. 4. Fig. 6 presents the XRD patterns of the immersed Ag/Cu/HA pellets, meaning that the formed new crystals are HA. As mentioned above, the stored crystal is more similar to nature bone in the respect of crystallinity and has a large dissolution rate. Consequently, during immersing, the Ag/Cu/HA crystals are partially dissolved in SBF at the start stage leading to an increase of concentrations of Ca^{2+}, PO_4^{3-} and OH^{-} near the surface of Ag/Cu/HA powders and HA is crystallized again from SBF, which is very similar to the mineralization of nature bone [29]. The

Table 5
The minimum inhibitory concentrations (MIC) of the four HAP against *E. coli.* and *S. aureus*.

Sample[a]	MIC[b]/$\times 10^{-3}$ ppm	
	Against *E. coli*	Against *S. mutans*
HAP	–[c]	–[c]
AgHAP	5	5
Cu/HAP	10	10
Ag/CivHAP	3.4	3.4
Ag/Cu/HAP[d]	3	3.1

[a] Sample calicined at 100 °C for 20 h.
[b] Minimum inhibitory concenteration.
[c] Without antibacterial property.
[d] After storing.

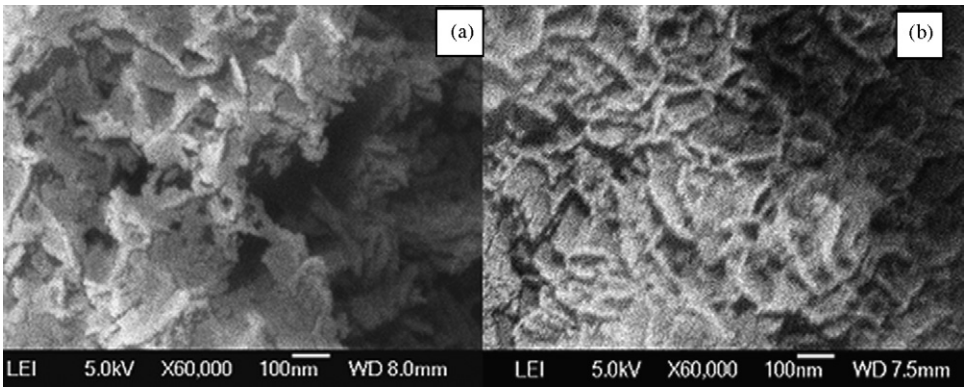

Fig. 5. The SEM micrograph of Ag/Cu/HA calcined at 600 °C after immersion in SBF: (a) before storing and (b) after storing.

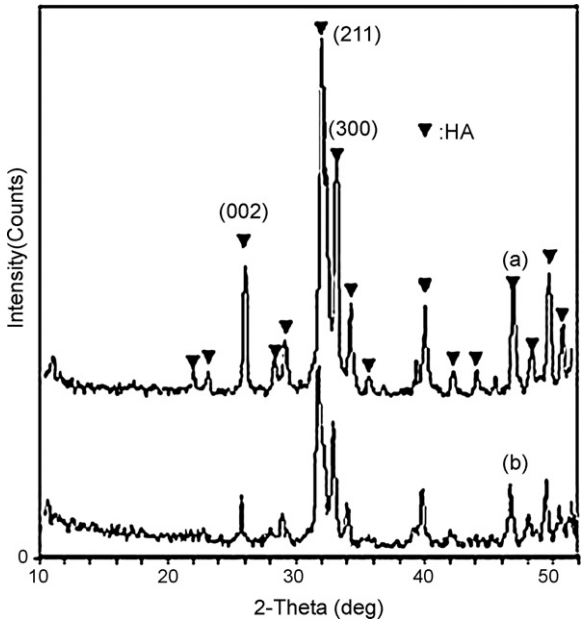

Fig. 6. The XRD patterns of the immersed Ag/Cu/HA in SBF: (a) before storing and (b) after storing.

new HA crystal shown by Fig. 5(b) has a smaller size and more uniform HA layer than Fig. 5(a) revealing that storing affects the microstructure of the new-formed HA. Fig. 5 also indicates that the new-formed HA has a platelet shape the same as the Ag/Cu/HA crystals. Fig. 6 obviously shows that the new-formed HA on the surface of un-stored crystal has higher intensity and crystallinity than that on the stored crystal. The change tendency of diffraction intensity and crystallinity is the same as that between the un-stored and stored Ag/Cu/HA crystals, which demonstrates that both stored and un-stored crystals can induce the formation and the orient growth of new HA crystals. The new HA layer on the stored crystal surface is more similar to nature bone because of its low diffraction intensities and crystallinity [29] than that on the un-stored crystal surface.

4. Conclusion

Considering the results mentioned above into account, we can draw the conclusion as follows: storing makes the diffraction intensities of the calcined Ag/Cu/HA powder reduced and the most significant reduction occurs in the sample calcined at 100 °C, meaning that storing decreases the crystallinity of the Ag/Cu/HA powder. Storing does not cause the Ag/Cu/HA nanoparticles to integrate but makes the sizes of the Ag/Cu/HA powder slightly changed. The decomposition of the $Ca_{19}Cu_2(PO_4)_{14}$ crystal at storing temperature makes the crystal's particle size reduce. The hydration of the ions on the surface of the Ag/Cu/HA crystal makes its small particle exist stably. Storing basically makes the diffraction angle of 0 0 2 and 3 0 0 peaks decrease but makes that of the 2 1 1 peak increase, causing the crystal lattice space to change. In addition, storing benefits the orient growth of the Ag/Cu/HA crystal along the direction of *c*-axis. The effects of storing on crystal morphology of the investigated Ag/Cu/HA powders are slight. The stored Ag/Cu/HA powders can induce the formation of new HA crystal, which is a weak crystal the same as the stored Ag/Cu/HA powders with platelet morphology and low diffraction intensity and crystallinity. The new HAP crystal is similar to nature bone. The Ag/Cu/HA crystals have more effective antibacterial property after storing than before storing.

Acknowledgements

This work was financially supported by the Key Research Item of Technology of Bureau of Science & Technology of Xi'an city, Shaanxi Province of China (Grant No. GG 200354) and partially supported by the Natural Science Foundation of Shaanxi Province of China (Grant No. 2004B24) and the Research Team Foundation of Shaanxi University of Science & Technology (sust-B104).

References

[1] L.L. Hench, E.C. Ethridge, Biomaterials, Academic Press, U.S.A., 1982.
[2] M. Yousefpour, A. Afshar, X. Yang, X. Li, B. Yang, Y. Wu, J. Chen, X. Zhang, Nano-crystalline growth of electrochemically deposited apatite coating on pure titanium, J. Electroanal. Chem. 589 (1) (2006) 96–105.
[3] K. Ioku, G. Kawachi, S. Sasaki, H. Fujimori, S. Goto, Hydrothermal preparation of tailored hydroxyapatite, J. Mater. Sci. 41 (5) (2006) 1341–1344.
[4] J.M. Crolet, M. Racila, R. Mahraoui, A. Meunier, A new numerical concept for modeling hydroxyapatite in human cortical bone, Comput. Methods Biomech. Biomed. Eng. 8 (2) (2005) 139–143.

[5] P. Laquerriere, A. Grandjean-Laquerriere, S. Addadi-Rebbah, E. Jallot, D. Laurent-Maquin, P. Frayssinet, M. Guenounou, MMP-2, MMP-9 and their inhibitors TIMP-2 and TIMP-1 production by human monocytes in vitro in the presence of different forms of hydroxyapatite particles, Biomaterials 25 (13) (2004) 2515–2524.
[6] K. Kandori, A. Fudo, T. Ishikawa, Study on the particle texture dependence of protein adsorption by using synthetic micrometer-sized calcium hydroxyapatite particles, Colloids Surf. B: Biointerfaces 24 (2) (2002) 145–153.
[7] P. Laquerriere, A. Grandjean-Laquerriere, M. Guenounou, D. Laurent-Maquin, P. Frayssinet, M. Nardin, Correlation between sintering temperature of hydroxyapatite particles and the production of inflammatory cytokines by human monocytes, Colloids Surf. B: Biointerfaces 30 (3) (2003) 207–213.
[8] N. Bouropoulos, J. Moradian-Oldak, Analysis of *Hydroxyapatite* Surface coverage by amelogenin nanospheres following the Langmuir model for protein adsorption, Calcified Tissue Int. 72 (5) (2003) 599–603.
[9] I. Yamaguchi, S. Iizuka, A. Osaka, H. Monma, J. Tanada, The effect of citric acid addition on chitosan/hydroxyapatite composites, Colloids Surf. A: Phys. Eng. Asp. 214 (1–3) (2003) 111–118.
[10] A.E. Porter, L.W. Hobbs, V.B. Rosen, M. Spector, The ultrastructure of the plasma-sprayed hydroxyapatie–bone interface predisposing, Biomaterials 23 (2002) 725–733.
[11] B. Chen, X.Y. Wu, X.H. Peng, Research on the layered microstructure of shankbone, Key Eng. Mater. 330–332 (II) (2007) 785–788.
[12] T. Kaneko, D. Ogomi, R. Mitsugi, T. Serizawa, M. Akashi, Mechanically drawn hydrogels uniaxially orient hydroxyapatite crystals and cell extension, Chem. Mater. 16 (2004) 5596–5601.
[13] M. Bellantone, N.J. Coleman, L.L. Hench, Bacteriostatic action of a novel four-component bioactive glass, J. Biomed. Mater. Res. 51 (2000) 484–490.
[14] A.G. Gristina, Biomaterial-centered infection: microbial adhesion versus tissue integration, Science 237 (1987) 1588–1595.
[15] J.J. Blaker, S.N. Nazhat, A.R. Boccaccini, Development and characterisation of silver-doped bioactive glass-coated sutures for tissue engineering and wound healing applications, Biomaterials 25 (7–8) (2004) 1319–1329.
[16] R.J. Chung, M.F. Hsieh, C.W. Huang, L.H. Perng, H.W. Wen, T.S. Chin, Antimicrobial effects and human gingival biocompatibility of hydroxyapatite sol–gel coatings, J. Biomed. Mater. Res. Part B: Appl. Biomater. 76 (1) (2006) 169–178.
[17] R.J. Chung, M.F. Hsieh, K.C. Huang, L.H. Perng, F.I. Chou, T.S. Chin, Anti-microbial hydroxyapatite particles synthesized by a sol–gel route, J. Sol–Gel Sci. Technol. 33 (2) (2005) 229–239.
[18] K.S. Oh, K.J. Kim, Y.K. Jeong, Y.H. Choa, Effect of fabrication processes on the antimicrobial properties of silver doped nano-sized Hap, Key Eng. Mater. 240–242 (2003) 583–586.
[19] J.D. Li, Y.B. Li, Y. Zuo, G.Y. Lu, W.H. Yang, L.R. Mo, Preparation and antibacterial properties valuation of copper-substituted nano-hydroxyapatite, J. Funct. Mater. 37 (4) (2006) 635–638 (in Chinese).
[20] B. Sutter, D.W. Ming, A. Clearfield, L.R. Hossner, Mineralogical, Chemical characterization of iron-, manganese-, and copper-containing synthetic hydroxyapatites, Soil Sci. Soc. Am. J. 67 (6) (2003) 1935–1942.
[21] T.N. Kim, G.L. Feng, J.O. Kim, J. Wu, H. Wang, G.C. Chen, F.Z. Cui, Antimicrobial effects of metal ions (Ag^{+}, Cu^{2+}, Zn^{2+}) in hydroxyapatite, J. Mater. Sci. Mater. Med. 9 (3) (1998) 129–134.
[22] S. Michiko, B.S. Elliott, J.W. Thomas, Enhanced osteoblast adhesion on hydrothermally treated hydroxy-apatite/titania/poly (lactide-co-glycolide) sol–gel titanium coatings, Biomaterials 26 (2005) 1349–1357.
[23] C.Z. Feng, Reference Book for Inorganic Chemistry, Higher Education Press, Beijing, 1985, pp. 27–55.
[24] W.J. Shaw, A.A. Campbell, M.L. Paine, M. Snead, The COOH Terminus of the amelogenin, LRAP, is oriented next to the hydroxyapatite surface, J. Biol. Chem. 279 (2004) 40236–40266.
[25] E. Rokita, P.A. Chevallier, P.H. Mutsaers, Z. Tabor, A. Wrobel, Studies of crystal orientation and calcium distribution in trabecular bone, Nucl. Instrum. Methods Phys. Res. Sect. B 240 (2005) 69–74.
[26] K. Yamauchi, N. Tadeuchi, H. Einaqa, T. Tanabe, Preparation of collagen/calcium phosphate multilayer sheet using enzymatic mineralization, Biomaterials 25 (24) (2004) 5481–5489.
[27] J.X. Zhang, M. Maeda, N. Kotobuki, M. Hirose, H. Ohqushi, D.L. Jiang, M. Iwasa, Aqueous processing of hydroxyapatite, Mater. Chem. Phys. 99 (2–3) (2006) 398–404.
[28] B. Chen, X.H. Peng, X.Y. Wu, Sheet-layer microstructure and toughness mechanism of shinbone, Key Eng. Mater. 334–335 (II) (2007) 1129–1132.
[29] M.J. Olszta, X.G. Cheng, S.S. Jee, R. Kumar, Y.Y. Kim, M.J. Kaufman, E.P. Douglas, L.B. Gower, Bone structure and formation: A new perspective, Mater. Sci. Eng. R 58 (2007) 77–116.